JOURNAL OF SURGICAL RESEARCH 183 (2013) 574–582

Available online at www.sciencedirect.com

SciVerse ScienceDirect

journal homepage: www.JournalofSurgicalResearch.com

Interleukin-17A plays a pivotal role in cholestatic liver fibrosis in mice

Michio Hara, MD, Hiroshi Kono, MD, PhD, Shinji Furuya, MD, Kazuyoshi Hirayama, MD, Masato Tsuchiya, MD, PhD, and Hideki Fujii, MD, PhD*

First Department of Surgery, University of Yamanashi, Yamanashi, Japan

ARTICLE INFO

Article history:
Received 18 October 2012
Received in revised form
20 February 2013
Accepted 7 March 2013
Available online 28 March 2013

Keywords:
Interleukin-17A
Interleukin-17A knockout mouse
Hepatic stellate cell
Kupffer cell
Bile duct ligation

ABSTRACT

Background: It was recently reported that serum interleukin (IL)-17 levels increased in liver fibrosis associated with human alcoholic liver disease. However, the role of IL-17 in liver fibrosis has not yet been elucidated. Therefore, the aim of this study was to evaluate the role of IL-17 on cholestatic liver fibrosis.

Materials and methods: IL-17A knockout (KO) and wild-type (WT) mice were subjected to bile duct ligation. Animals were sacrificed at designated times, and serum and liver tissues were collected. The mRNA expression of hepatic fibrotic markers was assessed, and distribution of activated hepatic stellate cells (HSCs) was determined by immunohistochemical staining. In an *in vitro* study, Kupffer cells (KCs) and HSCs were isolated from WT mice. KCs were cultured with IL-17A or IL-17F, and production of tumor necrosis factor α (TNF-α) and transforming growth factor β1 (TGF-β1) was measured. HSCs were cultured with IL-17A or IL-17F, and morphologic changes were assessed by immunohistochemical staining.

Results: Liver damage observed in the WT mice was significantly improved in the KO mice. Serum TNF-α and TGF-β1 levels were significantly decreased in the KO compared with the WT mice. The hepatic mRNA expression of TNF-α, TGF-β1, and collagen 1α1, which increased in the WT mice, also significantly decreased in the KO mice. Increased hepatic fibrosis in the WT mice was significantly improved in the KO mice. Cytokine production was increased in IL-17A-treated KCs. The most remarkable myofibroblast-like changes were observed in isolated HSCs in the presence of IL-17A.

Conclusions: IL-17A was involved in the pathogenesis of cholestatic liver fibrosis by activation of both the KCs and HSCs.

© 2013 Elsevier Inc. All rights reserved.

1. Introduction

Liver fibrosis is commonly caused by chronic liver disease, and it increases the risk of liver cancer and can ultimately result in death by liver failure [1,2]. The causes of hepatic fibrosis include viral infection, parasitic infection, alcohol, autoimmunity disorders, allergies, and chemical substances. In addition, recently, nonalcoholic steatohepatitis has arisen as one important cause of hepatic fibrosis. In certain diseases, treatment includes eliminating the causes; however, once the accelerator for the fibrogenesis has been taken, fibrosis progresses regardless of the cause. Effective treatment for liver fibrosis has not yet been established, except for liver transplantation [1,2]. On this point, investigation of the

* *Corresponding author*. First Department of Surgery, Faculty of Medicine, University of Yamanashi, 1110 Shimokato, Chuo, Yamanashi 409-3898, Japan. Tel./fax: +81 (0)55 273 7390.
E-mail address: hkouno@yamanashi.ac.jp (H. Kono).
0022-4804/$ – see front matter © 2013 Elsevier Inc. All rights reserved.
http://dx.doi.org/10.1016/j.jss.2013.03.025

mechanisms of fibrogenesis is important for establishing new therapies.

The activated hepatic stellate cell (HSC) plays a pivotal role in hepatic fibrogenesis. Activation of HSCs was caused by interaction with the Kupffer cell (KC), the sinusoidal endothelial cell, and the hepatocyte [3–6].

Interleukin (IL)-17A was originally described and cloned by Rouvier *et al*. and named cytotoxic T lymphocyte–associated serine esterase-8 (CTLA8) [7]; it was subsequently renamed IL-17, and six subtypes (IL-17A–F) were described [8]. Furthermore, it was reported from this laboratory that the IL-17 is involved in the pathogenesis of bacterial peritonitis and hepatic ischemia-reperfusion injury [9,10]. In those reports, IL-17A induced tumor necrosis factor α (TNF-α) production by the isolated Kupffer cell. Moreover, IL-17 has been reported to be involved in human alcoholic liver disease [11]. Thus, IL-17 plays a pivotal role in inflammatory conditions; however, the role of IL-17A in hepatic fibrosis due to inflammation is still unknown.

A previous study reported the important role of IL-17 in IL-17 receptor–deficient mice [12]. IL-17A and IL-17F have a common receptor; therefore, they are considered to have a similar effect [13–15]. The difference between the functional role of IL-17A and that of IL-17F still has not been fully elucidated. The specific purpose of the present study was to investigate the role of IL-17A in cholestatic liver fibrosis using the bile duct ligation (BDL) model in IL-17A knockout (KO) mice.

2. Materials and methods

2.1. Bile duct ligation model

Male wild-type (WT) mice (C57BL/6, 10–12 wk of age, obtained from Jackson Laboratories, Bar Harbor, ME) and IL-17A KO mice (backcrossed onto C57BL/6) were housed in a clean, temperature-controlled environment with a 12-h light-dark cycle and were given free access to regular laboratory chow diet and water for several days. All animals received humane care, and the study protocols were approved by the Committee of Laboratory Animals at the University of Yamanashi according to institutional guidelines.

The WT and IL-17A-KO mice were subjected to double ligation of the common bile duct (BDL). Briefly, mice were anesthetized with inhaled diethyl ether. After an upper midline laparotomy (15 mm), the common bile duct was exposed and ligated two times with nonabsorbable 6-0 monofilament sutures. The abdomen was closed with 3-0 braided silk sutures in layers.

Blood samples were collected *via* the inferior vena cava at 7 d and 14 d after the BDL or sham operation. The samples were centrifuged at 1200 *g* for 10 min at 4°C, and serum was stored at −80°C until assay.

Tissue samples were also collected at 14 d after the BDL or sham operation and were stored at −80°C for further analysis. Samples were fixed in formalin, embedded in paraffin, and serially sectioned. Some sections were stained with hematoxylin-eosin to assess inflammation and necrosis. The sections were evaluated in a blind manner by one of the authors and by an expert in rodent pathology.

2.2. Measurement of serum alanine aminotransferase

Blood samples were collected *via* the inferior vena cava at 7 d and 14 d after the BDL or sham operation ($n = 6$ for each time point). The samples were centrifuged at 1200 *g* for 10 min at 4°C, and serum was stored at −80°C. Serum alanine aminotransferase (ALT) levels were measured to assess hepatic parenchymal damage using FUJI DRI-CHEM analyzers (Fujifilm Co, Tokyo, Japan).

2.3. Measurement of serum cytokines

Blood samples were collected *via* the inferior vena cava at 7 d and 14 d after the BDL or sham operation ($n = 6$ for each time point). The samples were centrifuged at 1200 *g* for 10 min at 4°C, and serum was stored at −80°C until the assays. Determination of serum TNF-α (R&D Systems, Minneapolis, MN) and transforming growth factor β1 (TGF-β1; eBioscience Inc, San Diego, CA) levels were measured using enzyme-linked immunosorbent assay (ELISA) kits.

2.4. RNA isolation and real-time polymerase chain reaction

Previously frozen liver tissue samples (~30 mg/mouse) were homogenized in 600 μL RLT buffer (Qiagen, Valencia, CA) containing 1% β-mercaptoethanol. The lysate was centrifuged for 3 min at 13,000 rpm. RNA was isolated using an RNeasy kit (Qiagen) as per the manufacturer's protocol. Total RNA (10 μg) was reverse-transcribed using random primers and the high-capacity cDNA archive kit (Applied Biosystems, Foster City, CA) according to the manufacturer's protocol. The resulting cDNA was stored at −20°C.

The following Taqman (Applied Biosystems) gene expression assays were used for quantitative real-time polymerase chain reaction (PCR): TGF-β1 (Mm01178820_m1), Collagen 1α1 (Col1α1; Mm00801666_g1), TNF-α (Mm00443258_m1), and 18s rRNA (no. 4310893E). Reactions were performed in a 96-well assay format. Each plate contained one experimental gene and a housekeeping gene. Each reaction contained 2 μL cDNA template, 20.5 μL RNase-free H_2O, 2.5 μL TaqMan gene expression assay primer, and 25 μL TaqMan universal PCR master mix (Applied Biosystems). Reactions were processed for 1 cycle of 2 min at 50°C and 10 min at 95°C, followed by 40 cycles of 15 sec at 95°C and 1 min at 60°C on the AB 7500 Real-Time PCR System (Applied Biosystems). The cycle threshold (Ct) for each sample was determined from the linear region of the amplification plot. The ΔCt value for TNF-α and TGF-β1 and Col1α1 relative to the control gene 18s rRNA was determined. The ΔΔCt values were calculated using treated group means relative to control group means. Fold change data were calculated from the ΔΔCt values.

2.5. Immunohistochemistry for α smooth muscle actin in the liver

The expression of α smooth muscle actin (α-SMA) in the liver was detected by immunohistochemical staining, as described elsewhere [16]. Briefly, formalin-fixed and paraffin-embedded tissue sections were deparaffinized. After incubation with

0.3% hydrogen peroxide to block endogenous peroxidase and subsequently with normal goat serum to inhibit nonspecific reactions, the sections were incubated with rabbit polyclonal to alpha smooth muscle actin antibody (Abcam, Cambridge, UK, 1:200 dilution) for 1 h at room temperature. Following incubation, immunoperoxidase staining was completed using a Vectastain ABC Elite kit (Vector Laboratories, Burlingame, CA) and diaminobentizine as a chromogen.

2.6. Quantitative analysis of hepatic fibrosis

The Sirius red staining and immunohistochemical staining of α-SMA were used for analysis of hepatic fibrosis. The area of hepatic fibrosis was calculated as means of the randomly selected five different fields in each liver sample, and indicated as a percentage of the total area of the field using PhotoShop and ImageJ software [17].

2.7. Isolation and culture of the Kupffer cells and assessment of TNF-α and TGF-β1 production

Kupffer cells were isolated from male C57BL/6J mice (10–12 wk old), as detailed elsewhere, with minor modifications [18]. Briefly, after mice were anesthetized with inhaled diethyl ether, the abdomen was opened, the portal vein was cannulated with a small length of polypropylene tube, the inferior vena cava was ligated above the diaphragm, and the inferior vena cava was dissected. The liver was perfused *in situ* for 5 min with Ca^{2+}/Mg^{2+}-free liver perfusion medium (LPM-1: 8000 mg/L NaCl, 400 mg/L KCl, 88.17 mg/L NaH_2PO_4-$2H_2O$, 120.45 mg/L Na_2HPO_4, 2380 mg/L HEPES, 350 mg/L $NaHCO_3$, 190 mg/L EDTA, 900 mg/L glucose, 6 mg/L Phenol red; pH 7.4, 37°C) and then was perfused with complete liver perfusion medium (LPM-2: same as LPM-1 except without EDTA and glucose, but with 560 mg/L $CaCl_2$-$2H_2O$; pH 7.4, 37°C) containing 0.06% collagenase type IV (Sigma, St. Louis, MO) for an additional 15 min. After perfusion, the liver was removed, cut into small pieces, and homogenized. After passing through a 70-μm nylon mesh to eliminate nondigested material, cells were washed twice with warm Gey's balanced salt solution (GBSS-B: 370 mg/L KCl, 210 mg/L $MgCl_2$-$6H_2O$, 70 mg/L $MgSO_4$-$7H_2O$, 150 mg/L NaH_2PO_4-$2H_2O$, 30 mg/L KH_2PO_4, 1090 mg/L glucose, 227 mg/L $NaHCO_3$, 225 mg/L $CaCl_2$-$2H_2O$, 6 mg/L Phenol red, 8000 mg/L NaCl, 100 U/L streptomycin, 105 U/L penicillin G; pH 7.4) and centrifuged over 16% (wt/vol) Nycodenz (Axis-Shields, Oslo, Norway) gradient for 20 min at 1900 *g* at 4°C. KCs were collected from under the interface, washed with GBSS-B, and resuspended at a concentration of 1×10^6 cells/mL in D-MEM media (Invitrogen, Carlsbad, CA). Isolated KCs were seeded (10^6 per well) in 24-well dishes and cultured in D-MEM media containing 10% fetal calf serum (FCS) for 12 h. After changing the media to remove the nonadherent cells, KCs were cultured with recombinant mouse (rm)IL-17A (R&D Systems) or rmIL-17F and lipopolysaccharide (LPS) to activate the KCs. Cultures were maintained for an additional 24 h, and the media were collected and stored at −80°C. Viability of the cells was confirmed by trypan blue exclusion and was >95% in all experiments.

TNF-α and TGF-β1 production from KCs into the medium was assayed using ELISA kits according to the manufacturer's protocol (Invitrogen). In all experiments, KCs were isolated from four different mice in each group.

2.8. Isolation and culture of the hepatic stellate cells

HSCs were isolated from male C57BL/6J mice (10–12 wk old; six mice were used for each isolation) using a modification of the methods of Baba *et al.* and Kawada *et al.* [19–21]. Isolated HSCs were collected and resuspended at a concentration of 1×10^6 cells/mL in D-MEM media and cultured on uncoated 24-well dishes (1×10^6 cells/well) in D-MEM media (Invitrogen).

2.9. Immunocytochemical analysis for cultured HSCs

Isolated HSCs were seeded at a density of 1×10^6 cells/mL in 24-well culture dishes and cultured in D-MEM media containing 10% FCS for 12 h. After washing in phosphate-buffered saline (PBS) to remove nonadherent cells, the cells were divided into three groups: (1) D-MEM (control), (2) D-MEM containing rmIL-17A (10 pg/mL), and (3) D-MEM containing rmIL-17F (10 pg/mL). Culture medium was changed every 48 h in each group. After incubation for 7 d, the adherent cells were washed with PBS. Subsequently, the cells were fixed with 4% paraformaldehyde fixative overnight at 4°C. After incubation with 0.3% hydrogen peroxide to block endogenous peroxidase and subsequently with normal goat serum to inhibit nonspecific reactions, the cells were incubated with rabbit polyclonal to alpha smooth muscle actin antibody (Abcam; 1:200 dilution) for 1 h at room temperature. Following incubation, immunoperoxidase staining was completed using a Vectastain ABC Elite kit (Vector Laboratories) and diaminobentizine as a chromogen. Quantitative analysis of the α-SMA-positive area was calculated from five different fields in each dish and indicated as a percentage of the total area of the field using PhotoShop and ImageJ software [17].

2.10. Hydroxyproline concentrations in culture medium of isolated HSCs

Isolated HSCs were seeded at a density of 1×10^6 cells/mL in 24-well dishes and cultured in D-MEM containing 10% FCS for 24 h. After preincubation, the cells were divided into the three groups, and the HSCs were co-cultured as previously described for 2 d. The supernatant hydroxyproline concentration was determined using ELISA kits according to the manufacturer's instructions (Cusabio Biotech Co, Ltd, Newark, DE).

2.11. Statistical analysis

Data are expressed as mean ± SD for the *in vivo* studies and as mean ± SEM for the *in vitro* studies. Statistical differences between mean values were analyzed by analysis of variance (ANOVA) with Bonferroni *post hoc* test. $P < 0.05$ was considered significant.

3. Results

3.1. Serum ALT levels after the BDL

Serum ALT levels (Fig. 1) did not increase in the sham operation groups. In contrast, in the BDL groups, serum ALT levels increased in both the WT mice (217.5 ± 48.1 IU/L) and the IL-17A KO mice (159.0 ± 88.5 IU/L) at 1 wk after the BDL.

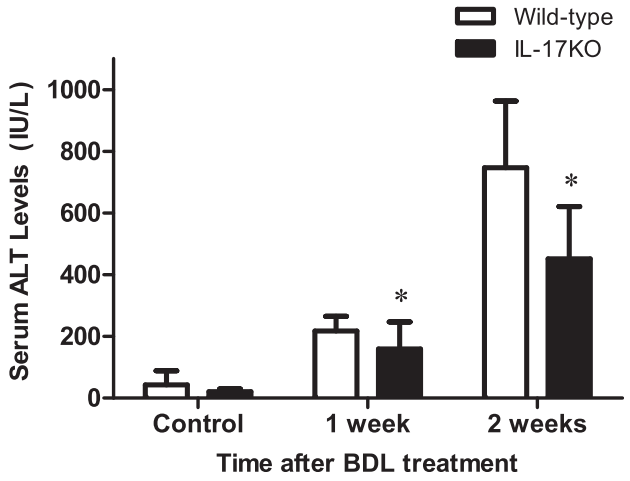

Fig. 1 – Serum ALT levels after BDL. Blood was collected *via* the inferior vena cava at 1 and 2 wk after BDL, and serum ALT levels were determined as described in Materials and methods. The values are mean ± SD ($n = 6$ in each group). *$P < 0.05$ compared with the WT mice by ANOVA with Bonferroni *post hoc* test.

Although the values were lower in the IL-17A KO mice than in the WT mice, the difference was not significant ($P = 0.112$). At 2 wk after the BDL, serum ALT levels were 747.0 ± 215.7 IU/L in the WT mice. In contrast, the values were significantly reduced by 40% in the IL-17A KO mice (451.0 ± 170.1 IU/L, $P = 0.018$).

3.2. *Serum cytokine levels after the BDL*

At 2 wk after the BDL, serum TNF-α and TGF-β1 concentrations (Fig. 2) increased in the WT mice (TNF-α: 67.3 ± 36.3 pg/mL; TGF-β1: 359.0 ± 46.3 pg/mL, respectively). On the other hand, these values were significantly decreased in the IL-17A KO mice (TNF-α: 33.3 ± 8.5 pg/mL, $P = 0.036$; TGF-β1: 306.6 ± 34.8 pg/mL, $P = 0.032$, respectively).

3.3. *mRNA expression of TNF-α, TGF-β1, and Col1α1 in the liver*

In the WT mice, the mRNA expression of TNF-α, TGF-β1, and Col1α1 (Fig. 3) increased 2 wk after the BDL (TNF-α: 1.24 ± 0.37; TGF-β1: 1.99 ± 0.38; Col1a1: 2.59 ± 0.93, respectively). However, the mRNA expressions of all three were significantly reduced in the IL-17A KO mice compared with the WT mice (TNF-α: 0.79 ± 0.23, $P = 0.038$; TGF-β1: 1.39 ± 0.44, $P = 0.017$; col1α1: 1.28 ± 0.47, $P = 0.010$, respectively).

3.4. *Histopathologic findings in the liver*

In the WT mice, the area of hepatocellular necrosis was greater than that in the IL-17A KO mice (Fig. 4A and B). To evaluate the fibrotic area in the liver, Sirius red staining and immunohistochemical staining for α-SMA were performed (Fig. 4C and D, and Fig. 5). Hepatic fibrosis was detected in the periportal area in the WT mice (Fig. 4C). In contrast, the fibrotic area was decreased in the IL-17 KO mice compared with the WT mice (Fig. 4D). Quantitative analysis of the Sirius red–positive area (Fig. 4E) showed a significant reduction of the fibrotic area in the IL-17 KO mice (3.66% ± 0.582%) compared with the WT mice (7.07 ± 0.83%, $P = 0.003$). Furthermore, similar results were observed in immunohistochemical staining for α-SMA (Fig. 5). Although the α-SMA-positive area was increased in both the WT mice (2.68% ± 0.16%) and the IL-17A KO mice (1.24% ± 0.22%) at 2 wk after the BDL, these values were significantly decreased (Fig. 5E) in the IL-17A KO mice compared with the WT mice ($P = 0.001$).

3.5. *Production of cytokines by isolated Kupffer cells*

Production of TNF-α and TGF-β1 was minimal in KCs incubated without LPS (Fig. 6A and B). After LPS stimulation, however, cytokine production increased markedly in cells treated with vehicle (TNF-α: 15.4 ± 0.64 pg/mL; TGF-β1: 1.67 ± 0.01 ng/mL, respectively). Although the production of these cytokines increased similarly in cells treated with rmIL-17A (TNF-α: 17.9 ± 0.75 pg/mL; TGF-β1: 1.78 ± 0.03 ng/mL, respectively) or rmIL-17F (TNF-α: 14.3 ± 1.05 pg/mL; TGF-β1: 1.67 ± 0.04 ng/mL, respectively), the production was significantly greater in cells treated with rmIL-17A.

3.6. *Expression of α-SMA in cultured hepatic stellate cells*

The expression of α-SMA was detected after 7 d in the HSCs cultured with control medium. This expression was increased

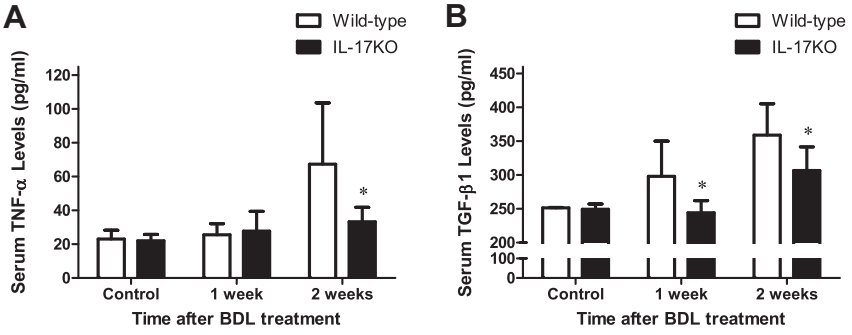

Fig. 2 – Serum cytokine levels after BDL. Serum TNF-α (A) and TGF-β1 levels (B) are shown. Blood was collected *via* the inferior vena cava at 1 and 2 wk after BDL, and serum TNF-α and TGF-β1 levels were determined as described in Materials and methods. Data represent mean ± SD ($n = 6$ in each group). *$P < 0.05$ compared with the WT mice by ANOVA with Bonferroni *post hoc* test.

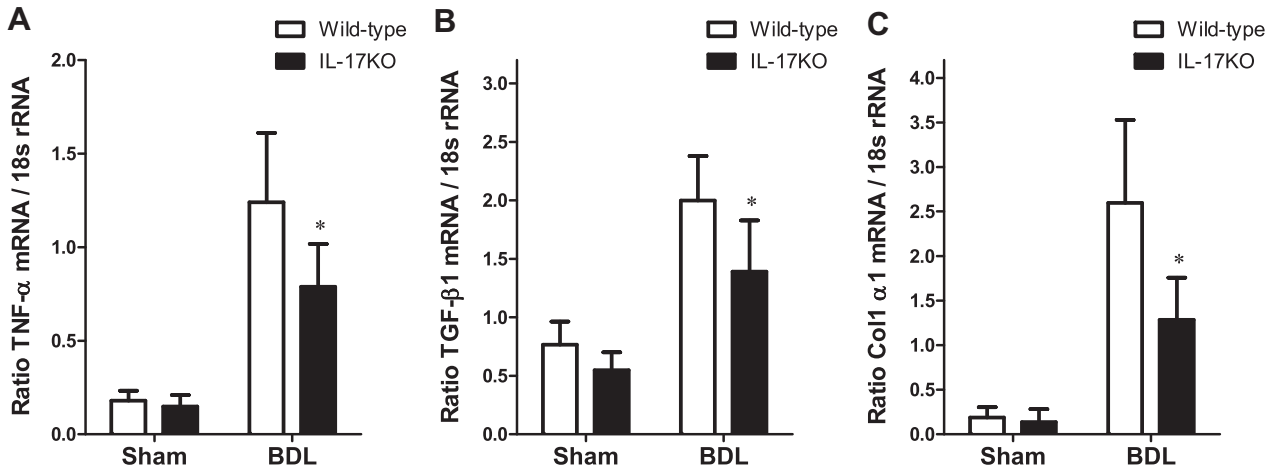

Fig. 3 – mRNA expression of liver by real-time RT-PCR. Mice underwent BDL or a sham operation, and total hepatic RNA was extracted after 2 wk. The mRNA expression of (A) TNF-α, (B) TGF-β1, and (C) Col1α1 was quantitated by real-time PCR and normalized as a ratio to 18s rRNA as a housekeeping gene. The mRNA expression was determined as described in Materials and methods. Data represent mean ± SD ($n = 6$ in each group). *$P < 0.05$ compared with the control group by ANOVA with Bonferroni *post hoc* test.

markedly by treatment with rmIL-17A or rmIL-17F compared with control medium (Fig. 7A–C).

Quantitative analysis of the α-SMA-positive area (Fig. 7D) assessed by image analysis showed significant expansion by about 1.5-fold greater in the cells with IL-17F compared with the cells incubated without IL-17F (49.2% ± 6.10% *versus* 31.7% ± 6.50%, $P = 0.008$). Furthermore, the area was 2.0-fold greater in the cells incubated with IL-17A compared with the cells incubated without IL-17A (62.9% ± 6.10% *versus* 31.7% ± 6.50%, $P < 0.001$).

3.7. *Production of hydroxyproline by isolated HSCs*

The concentration of hydroxyproline (Fig. 7E) was 2.80 ± 0.21 ng/mL in culture medium in the HSCs cultured with control medium for 2 d. There was no significant difference in hydroxyproline concentration between the control medium group and the group cultured in medium containing rmIL-17F (2.71 ± 0.29 ng/mL). On the other hand, the concentration of hydroxyproline was 3.35 ± 0.12 ng/mL in the cells incubated with rmIL-17A. There was a significant difference between the

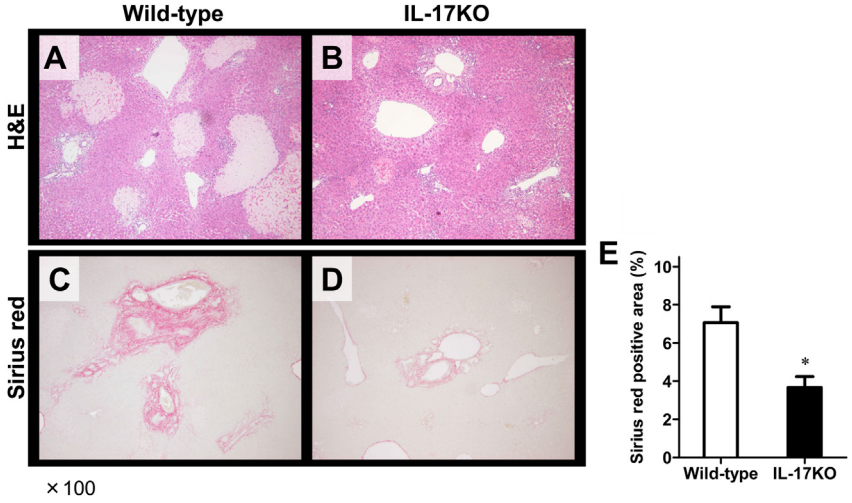

Fig. 4 – Pathologic findings in the liver after BDL. Livers were harvested from mice 2 wk after BDL or the sham operation as described in Materials and methods. (A) Hematoxylin-eosin staining in the livers from WT mice after BDL; (B) hematoxylin-eosin staining in the livers from IL-17A KO mice after BDL; (C) Sirius red staining in livers from WT mice after BDL; (D) Sirius red staining in livers from IL-17A KO mice after BDL. Representative photomicrographs are shown. Original magnification: ×100. (E) Quantitative analysis of Sirius red–positive area was calculated from five different fields in each liver sample, and the percentage of positive area per field is shown. Data represent mean ± SE ($n = 6$ in each group). *$P < 0.05$ compared with the WT mice by ANOVA with Bonferroni *post hoc* test.

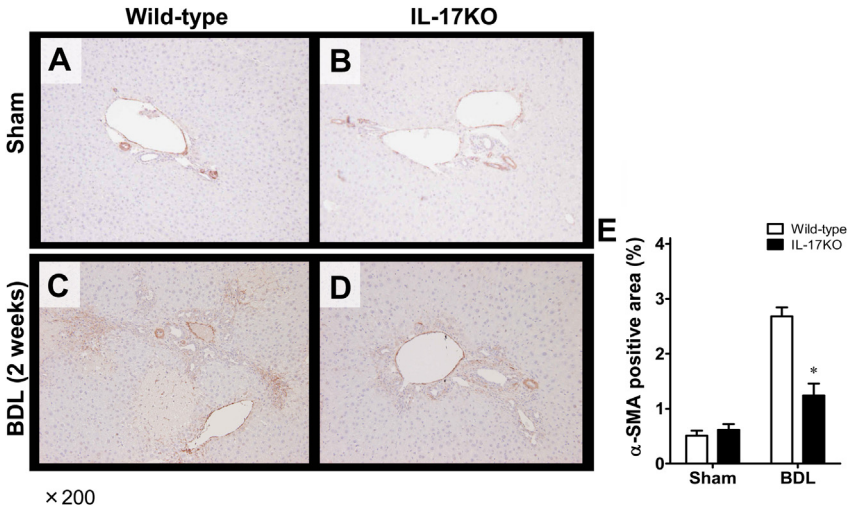

Fig. 5 – Immunohistochemical staining for α-SMA after BDL. Immunohistochemical staining was performed as described in Materials and methods. (A) Livers from WT mice after sham operation; (B) livers from IL-17A KO mice after BDL; (C) livers from WT mice after sham operation; (D) livers from IL-17A KO mice after BDL. Representative photomicrographs are shown. Original magnification: ×200. (E) Quantitative analysis of α-SMA-positive area was calculated from five different fields in each liver sample, and the percentage of positive area per field is shown. Data represent mean ± SE ($n = 6$ in each group). *$P < 0.05$ compared with the WT mice by ANOVA with Bonferroni *post hoc* test.

controls ($P = 0.026$) and cells cultured in medium containing rmIL-17F ($P = 0.038$).

4. Discussion

4.1. *Role of IL-17A in liver fibrosis*

Lemmers *et al.* reported that plasma IL-17 levels increase dramatically in alcoholic liver disease [11]. Furthermore, peripheral blood mononuclear cells produce higher amounts of IL-17 in patients with alcoholic liver disease. Thus, IL-17 contributes to inflammation.

On the other hand, development and progression of liver fibrosis are induced by inflammatory cytokines and oxidative stress [22,23]. These inflammatory cytokines are mainly produced by the hepatic macrophages, KCs. KCs are activated by oxidative stress or LPS derived from intestinal bacteria and produce inflammatory cytokines such as TNF-α, IL-6, and IL-1β. In the present study, cytokine levels of TNF-α and TGF-β1

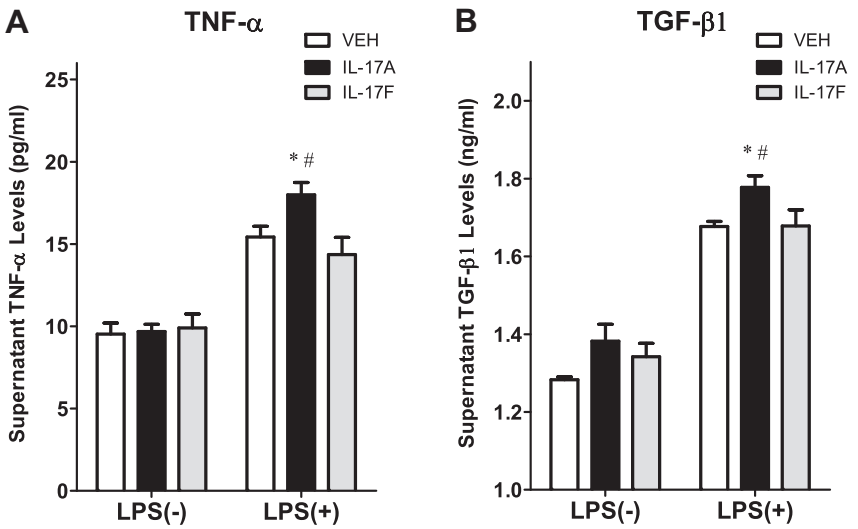

Fig. 6 – Production of cytokines by isolated Kupffer cells (TNF-α, TGF-β1). Kupffer cells were isolated from C57BL/6N mice and cultured in 24-well uncoated plastic plates for 24 h with rmIL-17A or rmIL-17F and LPS to activate the Kupffer cells. Production of TNF-α and TGF-β1 was determined as described in Materials and methods. (A) Supernatant TNF-α levels; (B) supernatant TGF-β1 levels. Data represent mean ± SE ($n = 4$ in each group). *$P < 0.05$ compared with the nontreated group by ANOVA with Bonferroni *post hoc* test. #$P < 0.05$ compared with the IL-17F-treated group by ANOVA with Bonferroni *post hoc* test.

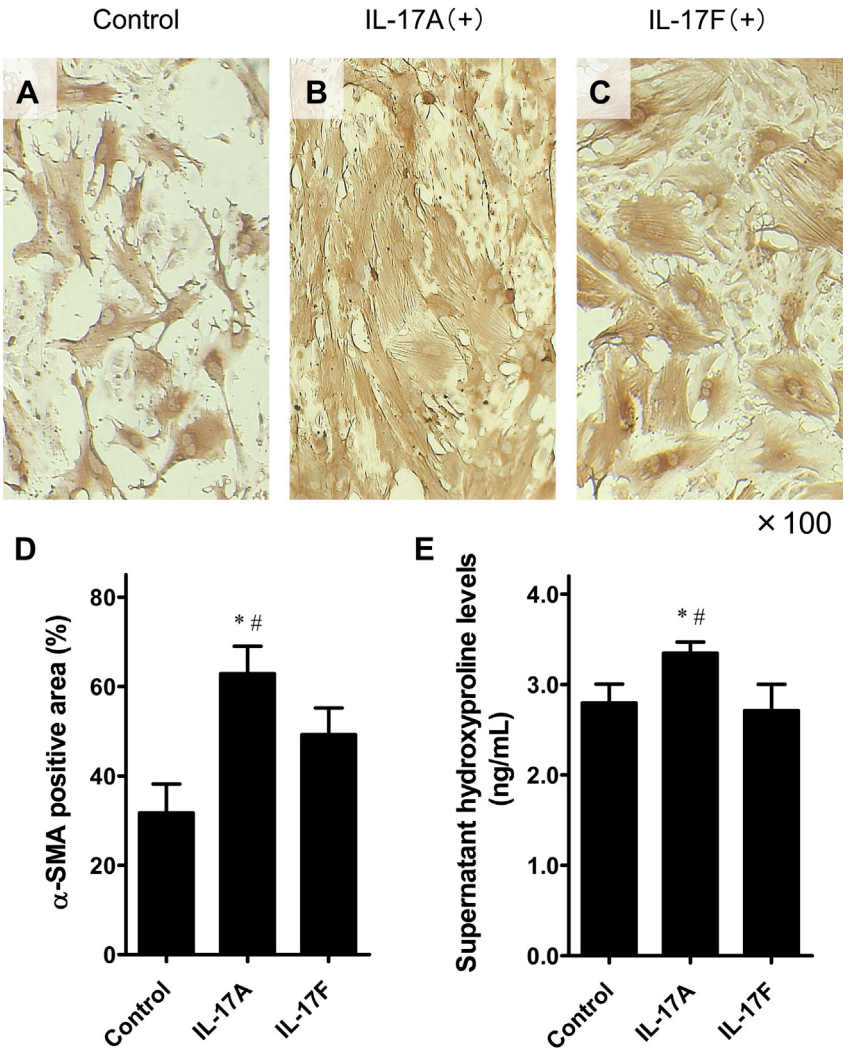

Fig. 7 – Effect of IL-17A and IL-17F on activation of HSCs. HSCs isolated from C57BL/6N mice were cultured in 24-well uncoated plastic plates for 24 h. Cells were divided into three groups: (A) control media; (B) IL-17A in media; and (C) IL-17F in media. HSCs were stained immunohistochemically using anti-α-SMA antibodies. Representative photomicrographs are shown. Original magnification: ×100. (D) Quantitative analysis of α-SMA-positive area was calculated from five different fields, and the percentage of positive area per field is shown. (E) Production of hydroxyproline by isolated HSCs. Data represent mean ± SE ($n = 4$ in each group). *$P < 0.05$ compared with control media by ANOVA with Bonferroni *post hoc* test. #$P < 0.05$ compared with media containing IL-17F by ANOVA with Bonferroni *post hoc* test.

were reduced in the IL-17 KO mice (Fig. 2). TNF-α is known to be involved in liver injury due to viral hepatitis and alcoholic hepatitis [24]. Plasma levels of TNF-α increase in patients with severe alcoholic hepatitis, and values correlate with the clinical course of the disease [25,26]. Iimuro *et al.* reported that in a rat enteral alcohol feeding model, treatment with antibodies to TNF-α protected against alcohol-induced liver injury [27]. Alternatively, TGF-β is another critical cytokine in fibrogenesis and inflammation [28]. Indeed, increased levels of TGF-β were observed in supernatants of isolated rat KCs after 10 wk of treatment with ethanol and a high-fat diet [29]. Therefore, TNF-α and TGF-β1 are considered to be important factors in inflammation and liver fibrogenesis.

The BDL model used in the present study is well characterized in regard to the nature of the hepatic injury [30]. In the present study, increases in the area of hepatic necrosis and levels of serum ALT in the WT mice were significantly reduced in the KO mice (Fig. 1). In the histologic findings, hepatic fibrosis observed in the WT mice was also improved in the KO mice (Figs. 4 and 5). This reduction in liver fibrosis seen in the KO mice was associated with suppression of cytokine levels of TNF-α and TGF-β1 and the mRNA expression of TNF-α, TGF-β1, and Col1α1 (Figs. 2 and 3). These findings indicate that the absence of IL-17A attenuates the inflammatory reaction and fibrogenesis.

4.2. *Effect of IL-17A on KCs and HSCs*

Activated KCs produce platelet-derived growth factor and TGF-β1, which induce activation of HSCs [31,32]. Activated

HSCs transform into myofibroblasts and play a central role together with KCs in the process of liver fibrosis through the production of collagen [4,33,34]. Therefore, the effect of IL-17A on KCs and HSCs was investigated in the present study. In the isolated KCs from WT mice, the production of TNF-α and TGF-β1 was increased in the KCs treated with rmIL-17A (Fig. 6). These results suggest that the KCs activated by IL-17A promote hepatic fibrosis.

In the present study, HSCs isolated from WT mice incubated with rmIL-17A or rmIL-17F were markedly transformed into myofibroblasts (Fig. 7). Furthermore, this phenomenon was more significant in the HSCs co-cultured with rmIL-17A than rmIL-17F. These results suggest that effects of IL-17A most likely include activation of KCs and/or HSCs.

In clinical cases, there are many different backgrounds such as hepatitis B virus, hepatitis C virus, and nonalcoholic steatohepatitis, and complications such as diabetes and hyperlipidemia often exist. Therefore, in the treatment of liver fibrosis, further examination would be required because the strategy for the treatment of the whole body or the whole organ is needed.

5. Conclusion

In the present study, hepatic fibrosis was prevented in the IL-17A KO mice. In the *in vitro* study, inflammatory cytokine production from KCs was increased by IL-17A stimulation. Furthermore, myofibroblast-like changes of HSCs were more enhanced in the presence of IL-17A. Thus, our data suggest that IL-17A rather than IL-17F plays a pivotal role in liver fibrosis due to cholestasis through the activation of KCs and HSCs.

REFERENCES

[1] Friedman SL. Mechanisms of disease: mechanisms of hepatic fibrosis and therapeutic implications. Nat Clin Pract Gastroenterol Hepatol 2004;1:98.
[2] Iredale JP. Models of liver fibrosis: exploring the dynamic nature of inflammation and repair in a solid organ. J Clin Invest 2007;117:539.
[3] Ballardini G, Fallani M, Biagini G, Bianchi FB, Pisi E. Desmin and actin in the identification of Ito cells and in monitoring their evolution to myofibroblasts in experimental liver fibrosis. Virchows Arch B Cell Pathol Incl Mol Pathol 1988;56:45.
[4] Friedman SL. Cellular sources of collagen and regulation of collagen production in liver. Semin Liver Dis 1990;10:20.
[5] Pinzani M, Rombouts K. Liver fibrosis: from the bench to clinical targets. Dig Liver Dis 2004;36:231.
[6] Bataller R, Brenner DA. Liver fibrosis. J Clin Invest 2005;115:209.
[7] Rouvier E, Luciani MF, Mattei MG, Denizot F, Golstein P. CTLA-8, cloned from an activated T cell, bearing AU-rich messenger RNA instability sequences, and homologous to a herpesvirus saimiri gene. J Immunol 1993;150:5445.
[8] Kolls JK, Linden A. Interleukin-17 family members and inflammation. Immunity 2004;21:467.
[9] Ogiku M, Kono H, Hara M, Tsuchiya M, Fujii H. Interleukin-17A plays a pivotal role in polymicrobial sepsis according to studies using IL-17A knockout mice. J Surg Res 2012;174:142.
[10] Kono H, Fujii H, Ogiku M, et al. Role of IL-17A in neutrophil recruitment and hepatic injury after warm ischemia-reperfusion mice. J Immunol 2011;187:4818.
[11] Lemmers A, Moreno C, Gustot T, et al. The interleukin-17 pathway is involved in human alcoholic liver disease. Hepatology 2009;49:646.
[12] Ye P, Rodriguez FH, Kanaly S, et al. Requirement of interleukin 17 receptor signaling for lung CXC chemokine and granulocyte colony-stimulating factor expression, neutrophil recruitment, and host defense. J Exp Med 2001; 194:519.
[13] Toy D, Kugler D, Wolfson M, et al. Cutting edge: interleukin 17 signals through a heteromeric receptor complex. J Immunol 2006;177:36.
[14] Zheng Y, Valdez PA, Danilenko DM, et al. Interleukin-22 mediates early host defense against attaching and effacing bacterial pathogens. Nat Med 2008;14:282.
[15] Iwakura Y, Nakae S, Saijo S, Ishigame H. The roles of IL-17A in inflammatory immune responses and host defense against pathogens. Immunol Rev 2008;226:57.
[16] Tanaka N, Kono H, Ishii K, Hosomura N, Fujii H. Dietary olive oil prevents carbon tetrachloride-induced hepatic fibrosis in mice. J Gastroenterol 2009;44:983.
[17] Miyazaki T, Karube M, Matsuzaki Y, et al. Taurine inhibits oxidative damage and prevents fibrosis in carbon tetrachloride-induced hepatic fibrosis. J Hepatol 2005;43:117.
[18] Tsuchiya M, Kono H, Matsuda M, Fujii H, Rusyn I. Protective effect of Juzen-taiho-to on hepatocarcinogenesis is mediated through the inhibition of Kupffer cell-induced oxidative stress. Int J Cancer 2008;123:2503.
[19] Baba S, Fujii H, Hirose T, et al. Commitment of bone marrow cells to hepatic stellate cells in mouse. J Hepatol 2004;40:255.
[20] Kawada N, Tran-Thi TA, Klein H, Decker K. The contraction of hepatic stellate (Ito) cells stimulated with vasoactive substances. Possible involvement of endothelin 1 and nitric oxide in the regulation of the sinusoidal tonus. Eur J Biochem 1993;213:815.
[21] Kojima-Yuasa A, Umeda K, Ohkita T, Opare Kennedy D, Nishiguchi S, Matsui-Yuasa I. Role of reactive oxygen species in zinc deficiency-induced hepatic stellate cell activation. Free Radic Biol Med 2005;39:631.
[22] Poli G, Parola M. Oxidative damage and fibrogenesis. Free Radic Biol Med 1997;22:287.
[23] Poli G. Pathogenesis of liver fibrosis: role of oxidative stress. Mol Aspects Med 2000;21:49.
[24] Schwabe RF, Brenner DA. Mechanisms of liver injury. I. TNF-alpha-induced liver injury: role of IKK, JNK, and ROS pathways. Am J Physiol Gastrointest Liver Physiol 2006;290: G583.
[25] McClain CJ, Cohen DA. Increased tumor necrosis factor production by monocytes in alcoholic hepatitis. Hepatology 1989;9:349.
[26] Felver ME, Mezey E, McGuire M, et al. Plasma tumor necrosis factor alpha predicts decreased long-term survival in severe alcoholic hepatitis. Alcohol Clin Exp Res 1990;14:255.
[27] Iimuro Y, Gallucci RM, Luster MI, Kono H, Thurman RG. Antibodies to tumor necrosis factor alfa attenuate hepatic necrosis and inflammation caused by chronic exposure to ethanol in the rat. Hepatology 1997;26:1530.
[28] Matsuoka M, Pham NT, Tsukamoto H. Differential effects of interleukin-1 alpha, tumor necrosis factor alpha, and transforming growth factor beta 1 on cell proliferation and collagen formation by cultured fat-storing cells. Liver 1989;9:71.
[29] Kamimura S, Tsukamoto H. Cytokine gene expression by Kupffer cells in experimental alcoholic liver disease. Hepatology 1995;22:1304.
[30] Canbay A, Higuchi H, Bronk SF, Taniai M, Sebo TJ, Gores GJ. Fas enhances fibrogenesis in the bile duct ligated mouse: a link between apoptosis and fibrosis. Gastroenterology 2002; 123:1323.

[31] Matsuoka M, Tsukamoto H. Stimulation of hepatic lipocyte collagen production by Kupffer cell-derived transforming growth factor beta: implication for a pathogenetic role in alcoholic liver fibrogenesis. Hepatology 1990;11:599.
[32] Tsukamoto H. Cytokine regulation of hepatic stellate cells in liver fibrosis. Alcohol Clin Exp Res 1999;23:911.
[33] Friedman SL. Molecular regulation of hepatic fibrosis, an integrated cellular response to tissue injury. J Biol Chem 2000;275:2247.
[34] Gressner AM. Transdifferentiation of hepatic stellate cells (Ito cells) to myofibroblasts: a key event in hepatic fibrogenesis. Kidney Int Suppl 1996;54:S39.